ORIGINAL RESEARCH

Preparation and characterisation of polycaprolactone–fibroin nanofibrous scaffolds containing allicin

Bita Mollaghadimi [ORCID]

Faculty of Biomedical Engineering– Biomaterials, Central Tehran Branch, Islamic Azad University, Tehran, Iran

Correspondence

Bita Mollaghadimi, Faculty of Biomedical Engineering– Biomaterials, Central Tehran Branch, Islamic Azad University, Tehran, Iran.
Email: bitamollaghadimi@gmail.com

Abstract

Polycaprolactone (PCL) and silk fibroin are used to make nanofiber wound dressings, and then allicin is added to PCL and silk fibroin to expand antibacterial properties. The polymer solutions are subjected to various electrospinning parameters, and allicin-containing and non-allicin fibres are prepared. Fibres are examined by scanning electron microscopy (SEM), Fourier-transform infrared spectroscopy (FTIR), contact angle analysis, mechanical testing, bacterial culture, and 3-(4 5-dimethylthiazol-2-yl)-2 5-diphenyltetrazolium bromide (MTT). The SEM results show that the addition of fibroin and allicin at a constant voltage provides a direct relationship between the distance and the diameter of the fibres. Also, the total variation algorithm is used for denoising the signal of FTIR that the results confirm the functional groups present in the fibres. Furthermore, the contact angle test for allicin-free fibres shows that the contact angle of these fibres is 133.3° that decreases to 85.5° by adding allicin to the structure. Moreover, the tensile test of allicin-free fibres shows that Young's modulus of these fibres is 2.06 MPa, while the value increases to 5.12 MPa with the addition of allicin to the structure and at the end of the bacterial culture test, a growth inhibition zone is seen after 17 and 24 h. According to the obtained results, these fibres have the potential to be used in burn applications.

1 | INTRODUCTION

Tissue engineering is a multidisciplinary field of principles and applications of engineering methods and life sciences. This fundamentally understands the relationship between structure and function in normal and abnormal tissues [1]. So far, tissue engineering has been used to repair many tissues, such as bone, cartilage, blood vessels, and skin. Tissue has several structural and mechanical properties to perform its function. To achieve this, tissue engineering uses cells placed inside an artificial support system. Cells are often implanted inside artificial structures that mimic and support the three-dimensional tissue structure. This structure is called a scaffold used both in vivo and in vitro [2, 3].

Bio-scaffolds are fabricated using biocompatible and degradable materials. The structure of these scaffolds should be as similar as possible to the texture of the implanting site. Thus, the reconstruction and healing of damaged tissue increase qualitatively and quantitatively. The scaffold structure is a porous matrix, which helps the cells connect an implant better. The size and intensity of porosity can be controlled. The main part of the work is a scaffold design, in which the size of pores, porosity intensity, and degree of degradability are determined. This ensures resistance to regional stresses until the time of destruction and uniformly distributes pressures in the whole implantation site [4]. Scaffolding is still used today to deliver medicine to its destination [5]. Lucas et al. used water-soluble proteins in the bovine bone to induce cartilage production and ossification. In this regard, polyanhydride was used to deliver these proteins to the desired destination [6].

Master et al. used a polymeric with a degradable polyanhydride matrix for long-term blockage but limited to specific areas so that drugs effective in thematic anaesthesia were released from it in a controlled manner and acted on the target area. A hybrid scaffold of polycaprolactone (PCL) polyvinyl alcohol with chitosan has been proposed in tissue engineering and biological implants [7]. PCL combination with other materials, such as Nigella sativa oil and anandamide, results in

leishmaniasis treatment [8, 9]. There are many purposes for the PCL. PCl was used for skin tissue in [10, 11] and wound healing in [12]. Also, the impressive improvement in flexibility of PCL was investigated in [13] that can be used for many applications in tissue engineering. In [14], PCL nanofibers were refined by halloysite nanotubes for tissue engineering. A novel electrospun nanofiber membrane was fabricated in [15] that consists of PCL, chitosan oligosaccharides, and Qe/Rutin as the potential bioactive dressing for wound healing that regardless other combinations was limited to poor water solubility [16]. In other applications, PCL was used for solid lithium batteries that have impressive advantage on cost and environmental friendliness. Their cells can even survive under several extreme conditions, such as bending, twisting, crimping, and stretching [16].

Nanofiber wound dressings may meet requirements, such as high gas penetration and wound protection against infection and dehydration. The purpose of the wound dressing is to produce an ideal structure that has good porosity and barrier to prevent the penetration of bacteria. To achieve this goal, wound dressings must be carefully selected, and the structure must be controlled to have all the appropriate properties and be impermeable to oxygen [17]. Through growth factors that mediate these pathways, cell adhesion and cell migration lead to wound healing. Skin regeneration is a complex process that involves the proliferation and alignment of cells where there is a barrier to regeneration [18]. One of the main barriers is the production of reactive oxygen elements from inflammation or infection. Spirulina is an aqueous green alga that has antioxidant and anti-inflammatory activities. In one nanofiber study, PCL compatibility with the spirulina extract was investigated as a wound dressing due to its antioxidant mechanism [19]. In addition to the increased viability of fibroblasts, the spirulina extract regulates internal and extracellular lining by increasing the antioxidant mechanism of fibroblasts. Finally, in vivo experiments confirmed that spirulina helps the wound to heal. Overall, the results of this study indicate that spirulina and nanofibers have the potential to be used in wound dressing to facilitate skin regeneration [20]. Nanofiber scaffolds have been used as one of the most critical tissue engineering scaffolds for wound healing [21]. Multifunctional nanofiber scaffolds with a mixture of viscous protein and polycaprolactone have previously been reported to have stable mechanical strength, be environmentally friendly, and have considerable ability to adsorb diverse bioactive molecules without any surface changes [22, 23]. In Kim et al.'s study, nanofibers with a mixture of bioactive molecules and PCL were used to heal skin wounds in vivo. The produced nanofibers helped regenerate and heal the wounds of mice quickly and created a very suitable environment for the growth of keratinocyte cells. Therefore, this study shows that scaffold adhesion properties can succeed in wound healing. Nanofibers and mixed bioactive molecules can also potentially be utilised for various tissue regeneration programs [24].

Venugopal et al. examined the wound dressings with polycaprolactone. Polycaprolactone has been studied primarily for long-term implants to release the drug into the body and support the formation of mineral-rich tissues. This may be a good choice for treating bone defects. Improving the mechanical properties of PCL is achieved by copolymerisation with polylactic acid. This allows it to be used for orthopaedic applications, such as repairing bone defects [25]. Polyurethane is used in wound dressing due to its properties and good permeability to oxygen. Nanofiber wound dressings may meet requirements, such as high gas penetration and wound protection against infection and dehydration. The purpose of the wound dressing is to produce an ideal structure that is an excellent barrier to prevent the penetration of harmful particles. To achieve this goal, wound dressings must be carefully selected, and their structure must be controlled [25]. Nanofiber scaffolding is one of the most critical tissue engineering scaffolds used for wound healing applications. Previously, electrospun nanofiber scaffolds with a mixture of viscous protein and polycaprolactone have been reported. Jebali et al. examined the stability, toxicity, and antimicrobial effects of soluble allicin. Their study investigates the antimicrobial properties of this solution on five mice about microbial properties and evaluates the toxicity on mouse skin cells. They also determine its stability at different time intervals [26].

Sardari et al. examined macroscopic aspects of earlier healing in deep wounds in five dog breeds. Tested wounds were treated topically with 0.5% allicin in methylcellulose gel, and control wounds were treated with methylcellulose gel only. Treatment began 24 h after injury. Wounds were evaluated over 4 weeks. Digital photos were taken of all the wounds on days 0, 3, 7, 10, 14, 17, 21, 24, and 28. As a reference, the rulers were held vertically and horizontally next to the wound [27]. Epithelialisation range and granular tissue were measured for each wound. The percentage of wound contraction, epithelialisation, and healing was calculated for each wound. Initially, the entire wound area grew large. After initial enlargement, wound areas in both test and control groups decreased rapidly [27].

In this paper, PCL, silk fibroin, and also allicin are used to make nanofiber wound dressings for expanding antibacterial properties that the proposed method is explained in the following.

2 | MATERIAL AND METHOD

Table 1 and Table 2 show a list of equipment and material required to conduct the lab activities under the study.

2.1 | Preparing silk, fibroin, and allicin

Allicin is derived from the garlic extract and can bind to thiol groups of proteins due to the thiosulfate group. This binding destroys various essential proteins and enzymes in microbes and can be effective against a wide range of viruses, bacteria, fungi, and parasites. Garlic is from the genus Alliaceae from the lily family and has been used as a medicine in ancient civilisations. The most crucial sulphur compound in garlic is allicin with a molecular weight of 162.3, which has antimicrobial and

T A B L E 1 Specifications of the equipment and devices used for fabrication and assessment of nanofiber scaffolds

| Description	Model
Electrospinning	Nanoazma
Stirrer	Isolab9001
Scale	Quintix313-15
Vacuum Oven	Memert
Centrifuge	SIGMA
Freeze dryer	Dena
Optical microscope	Nikon
SEM	DSM-960A
FTIR	PERKIN-ELMER
Mechanical properties test	SANTAM
Contact angle test	Fanavari Ezdiad Bardasht Fars

Abbreviation: FTIR, Fourier transform infrared.

T A B L E 2 Materials under the study

Description	Model
Polycaprolactone	SIGMA
Formic acid	Merk
Lithium bromide	Merk
Sodium carbonate	Merk
Dialysis membrane	Merk
silkworm cocoon	Silkworm Research Centre

therapeutic properties of garlic [28]. Allicin is a molecule that dissolves insignificantly in aqueous solutions. One of the essential properties of allicin is its ability to permeate and pass-through membrane phospholipids. This allows it to pass freely through the membrane and exert its effects. Allicin is produced by the action of the allicin enzyme from the allicin molecule. As existed in garlic, this enzyme is released by cutting, crushing, chewing, slicing, or extracting it and causes it to slip and turn into a sulfonic acid called allicin or diallyl thiosulfonate [29]. An example is the inhibition of acetylcholine. The inhibition of this enzyme prevents the biosynthesis of lipids and fatty acids and ultimately inhibits cell viability [30]. Although allicin has antimicrobial properties, it also affects the normal cells of the human and animal body [31].

In order to prepare allicin, 150 g of grated garlic was added to 1 L of distilled water. The mixture was then placed in a Clevenger at 70°C to reach the boiling point. During this process, the temperature was adjusted to 60°C. After 3 h, some outputs were obtained that these procedures are shown in Figure 1. In the next step, silk resin and fibroin purification are done based on following steps:

- Cutting silkworm cocoons.
- Accurately weighing the cocoons to the required amount.
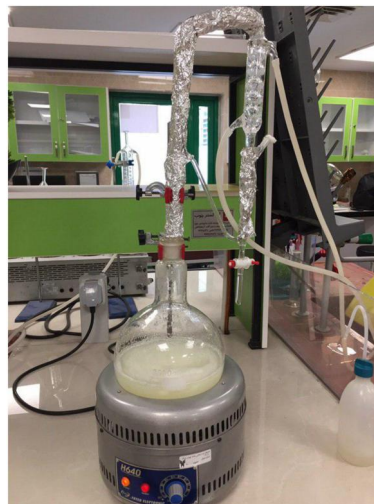
F I G U R E 1 Preparing allicin using Clevenger at 70°C

- Boiling in 0.02 M sodium carbonate solution for 1 hour.
- Washing with water and drying sericin-free silk.
- Dissolving the resulting fibres in lithium bromide for 4 h.
- Dialysing against deionised water for 48 h; new deionised water was replaced six times during dialysis.
- Centrifuging the solution at 9000 g for 20 min.
- Finally, after two centrifuges, the surface solution was purified as fibroin in a freeze-dryer for 48 h.

To prepare polymer solutions for electrospinning, specific amounts of PCL or silk fibroin (SF) were weighed and dissolved in the formic acid solvent. The solution was then placed on a stirrer at 300 rpm for 1 hour. Selected concentrations for PCL and SF solution were 20% and 10% by weight/volume, respectively. The variables required for scaffolding construction are voltage (kV), distance (cm), and flow rate (ml/h) that are adjusted in the device. Regarding the concentration variable, different ratios of PCL/SF with values of 90/10, 70/30, and 50/50 were examined. Finally, the ratio of 70/30 was selected according to the morphology of the resulting fibres.

2.2 | SEM, FTIR, and contact angle of the scaffolds analysis

Scanning Electron Microscope (SEM) is one of the most popular types of electron microscope that has found many applications in nanotechnology. The construction of the SEM allowed researchers to study the samples more simply and clearly. Electron beam bombardment of the sample causes electrons and photons to be released from the sample and sent to the detectors, where they are converted into signals. The movement of the beam on the sample provides a set of signals on the basis of which the microscope can display the cross-sectional image of the sample surface on the screen moment by moment. Initially, the main advantage of the SEM device

was the ability to obtain microscopic images directly from solid samples with a better resolution and focus compared to optical microscopes. But later it developed the executive and operational power and was equipped with analysis methods, such as X rays to determine the chemical composition and electronic channels to detect the crystalline state. To study the morphology of the samples, the scaffolds were cut in 1×1 cm2 and placed in a gold coating machine. Then, images were taken from it in different magnifications. To determine the fibre diameter from the SEM images, other image points are selected and finally averaged. Imagej software was used to determine the fibre diameter. SPSS or Excell software was used for statistical analysis. Then, the mean of the numbers was obtained, and the result was reported as mean ± standard deviation.

The FTIR analysis is based on the absorption of radiation and excitation at the vibrational energy levels of polyatomic molecules and ions. The electromagnetic waves used in vibrational spectroscopy are typically infrared light. Everything is constantly vibrating in the world around us, which is a direct result of the vibration of its constituent molecules. Molecular vibrations, in turn, are caused by oscillations in the bonds that make up a molecule. The wavenumber of each peak indicates the presence of a specific functional group in the sample. The location of the absorption peak of different functional groups has been collected in various books and various references, such as [32, 33].

Recently, a lot of research studies have been conducted on the behaviour of drops in contact with surfaces. These studies were mainly based on fluid dynamics. Its applications include thin coating, spray paint, application in pesticides, and plasma spraying. In general, the behaviour of the droplet is a function of the properties of the droplet, the surface, and the environment. The contact angle is one of the defining parameters of this behaviour. The contact angle of the droplet with the surface has been used to describe wetting, solid surface, condensation and evaporation, removal of frost, adhesion between droplets and solid surfaces, and many other practical applications. Hence, accurate contact angle measurement is essential not only for scientific research but also for a wide range of industrial applications. In this line, a drop of 5 ml of water was placed on each of the scaffolds with the help of a dropper and then, with the use of a Dino digital camera, the image was taken.

2.3 | Denoising FTIR

Total variation regularisation is used for noise reduction in digital image processing and werable sensors [34–43]. Total variation (TV) is integral to the absolute gradient of the digital signal and possesses a high value [34–37]. Original signal (without noise) can be obtained by decreasing the total variation of the digital signal [35–39]. In order to denoise the obtained signal, a method is proposed based on a function, which is called the TV algorithm. This function attempts to minimise Eq. (1).

$$\min_{x,\mu} \frac{\mu}{2}\|f - g\|^2 + \|Df\| \tag{1}$$

where μ and D are regularisation parameter and first-order forward finite difference operator, respectively. f and g are the FTIR data before and after denoising.

2.4 | Tensile test

A tensile test was performed by Instron tensile testing device (model 5566, made in England). The preparation of tensile test specimens is as follows. The samples were cut to dimensions of 3×4 cm, and each was pasted on a paper of specific dimensions. Samples with these conditions were placed in the jaw of the device, which had a speed of 2 mm/min. Then, the specimens were pulled until rupture occurred. Finally, the size of the elastic modulus of the scaffolds was determined from the slope of the line of the elastic region on the curves. The results were first evaluated for the PCL tensile test. The sample specimens were a rectangle 9 mm wide, gauge length 20 mm, and thickness 0.09 mm at a speed of 5 mm/min.

2.5 | Cytotoxicity test

To investigate the toxicity of the samples and the effect of the samples on cell growth and proliferation, the extraction process of scaffolds was performed. Extraction was performed at 37°C at intervals of 1 and 4 days. A toxicity test was performed according to ISO10993-5. 3-(4 5-dimethylthiazol-2-yl)-2 5-diphenyltetrazolium bromide (MTT) is a water-soluble yellow tetrazolium salt. Metabolically active cells have pigmentation properties in water-soluble dark blue formazan by cleaving the tetrazolium ring. The scaffolds were sterilised by ultraviolet radiation for half an hour. MG63 cells were used in this study. Cells with an initial density of 1x104 in each well were exposed to a Dulbecco's Modified Eagle Medium culture medium in a 24-well plate. Then, extracts from sterilised scaffold samples were poured into each well. After 1 and 4 days, an MTT assay was performed to evaluate cell viability. For this purpose, after draining the medium and washing with PBS, 100 µl of MTT solution (5 mg/ml) was added to each culture well. Then, it was kept in an incubator at 37°C for 4 h. Then, the medium was slowly drained, and dimethyl sulfoxide (DMSO) was added to the well to dissolve the formazan. The light absorption was read at 570 nm. A similar procedure was performed for MG63 cells in a culture medium without scaffold samples as a control.

2.6 | Bacterial culture test and evaluation of antibacterial properties

Standard strains of gram-negative and gram-positive bacteria, including Escherichia coli and Staphylococcus aureus, were used in this test. Experiments were performed on both gram-

negative and gram-recorded groups. An agar nutrient microbial culture medium was prepared. Then, the bacteria were cultured on the medium. After disk diffusion, the Petri dishes were incubated at 37°C for 24 h. Then, the growth inhibition zone diameter was measured using an accurate ruler. Nanofibers with and without allicin were examined in this test. Note that the nanofibers were cut into a circle with a diameter of 5 mm and sterilised by ultraviolet light for 20 min.

3 | RESULTS AND DISCUSSIONS

In this section, the results and analyses for the scaffolds are tested, separately.

3.1 | SEM results

The SEM analysis is used to study the morphology of PCL nanofibers, PCL/SF containing and free of allicin that the obtained results are as follows:

3.1.1 | Effect of collector rpm on morphology and diameter of PCL nanofibers

According to the SEM images (Figure 2) for PCL fibres prepared from 20% solution, the diameter of scaffold nanofibers was calculated and presented in Table 3. For the PCL solution prepared from 20% formic acid, all electrospinning parameters were fixed, and rpm varied to reduce the diameter of the fibres. Electrospinning parameters, including a constant distance, were considered throughout the experiment (22 cm), and also a constant voltage of 20 kV was set. Based on the results of Table 3 and zero rpm, the diameter of the nanofibers at a concentration of 20% was 221.1 ± 1.9 nm. To reduce the diameter of the nanofibers, the rpm was increased at a concentration of 20% to 100 and 300 rpm. As the collector rpm was increased to 100 and 300, the nanofiber diameters reached 182 ± 1.1 and 173.5 ± 1.2 nm, respectively. The concentration was reduced from 20% to 15%, and a voltage of 20 kV was applied to reduce the diameter. Under these conditions, fibres

were obtained with many beads. Therefore, the voltage was reduced from 15 to 12 kV at a concentration of 15%, which will be thoroughly discussed in the next section.

### 3.1.2 | Effect of concentration reduction on nanofiber diameters

Considering the SEM images for nanofibers obtained from 15% PCL solution (Figure 3), Table 4 reports the relevant parameters. As shown in Table 4 for the PCL solution in 15% formic acid, the experiments were performed at a fixed distance of 20 cm. Also, the voltage test was constant, equal to 12 kV. As can be seen, the nanofiber diameter for this sample was zero at 201.2 ± 1.3 nm. At the same time, this value was determined 119.7 ± 2.1 nm at 100 times. At 300 rpm, the fibre diameter was 122.4 ± 1.5 nm. This nanofiber diameter was determined based on an average of 10 images. With increasing speed from 0 to 300, a significant decrease in diameter was first seen in nanofibers from 0 to 100. Then, from 100 to 300 rpm, an insignificant increase in the diameter of the nanofibers was observed.

### 3.1.3 | Effect of fibroin on the nanofiber diameter

SEM images for adding SF to PCL and producing PCL/SF fibres are shown in Figure 4. As it can be seen, the diameter of PCL/SF fibres can be obtained with the help of Image J software. For this purpose, several cases are considered from each image (a–c) for each case. For example, Figure 4a has eight images for which the

TABLE 3 Distance, voltage, and diameter of PCL solution nanofibers with 20% formic acid

Distance (cm)	Voltage (kV)	Fibre diameter (nm) (nm)	Sample code
22	20	221.1 ± 1.9	$PCL20_0$
22	20	182 ± 1.1	$PCL20_{100}$
22	20	173.5 ± 1.2	$PCL20_{300}$

(a)   **(b)**   **(c)**
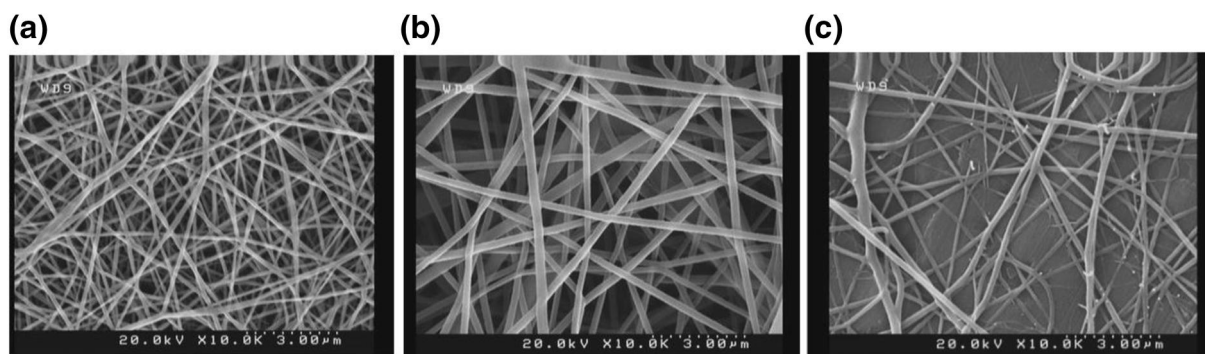
FIGURE 2 SEM images related to PCL solution nanofibers with 20% formic acid in various collector rpms: (a) 0, (b) 100, and (c) 300
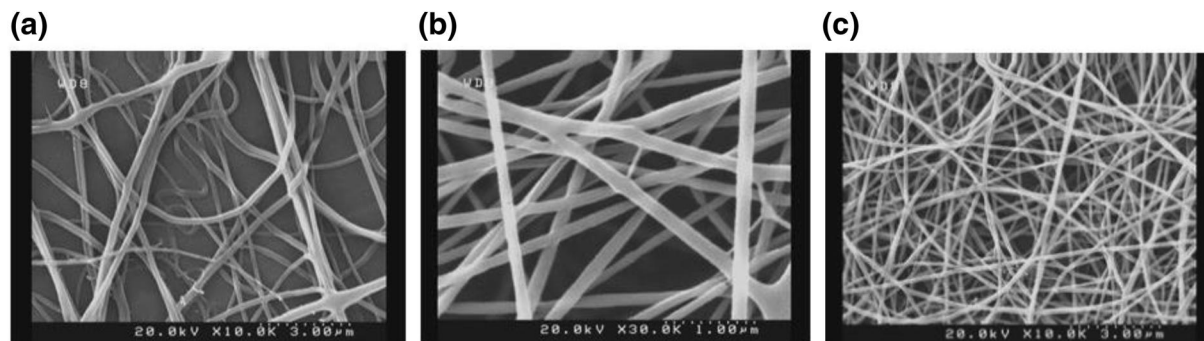
FIGURE 3 SEM images related to PCL solution nanofibers with 15% formic acid in various collector rpms: (a) 0, (b) 100, and (c) 300

TABLE 4 Distance, voltage, and diameter of PCL solution nanofibers with 15% formic acid

Distance (cm)	Voltage (kV)	Fibre diameter (nm) (nm)	Sample code
20	12	201.2 ± 1.3	$PCL15_0$
20	12	119.7 ± 2.1	$PCL15_{100}$
20	12	122.4 ± 1.5	$PCL15_{300}$

average SEM is considered. The results of Table 5 are explained as follows. If the distance is fixed, increasing the voltage from 15 to 20 kV reduces the diameter of PCL/SF nanofibers from 104.7 ± 1.1 nm to 100.2 ± 0.9 nm. If the voltage is fixed to 20 kV, increasing the distance from 15 to 18 cm reduces the diameters of PCL/SF nanofibers from 100.2 ± 0.9 nm to 98.1 ± 2.1 nm. By increasing the voltage and electric field power, the electrical charge of the polymer chain will be increased in the jet, leading to increased repulsive force between the chains, and as a result, reduced diameter of nanofibers. However, this reduction is not significant ($P > 0.05$).

### 3.1.4 | Effect of allicin on nanofiber diameters

SEM images for adding allicin to SF and PCL are shown in Figure 5. According to the test conditions, Figure 5a shows a voltage of 15 kV and a distance of 15 cm. Figure 5b indicates a test at 20 kV and a distance of 15 cm, and Figure 5c presents a test at 20 kV and a distance of 18 cm. Electrospinning conditions are given in Table 6. The fibre diameter was calculated from each sample code before using the Image J software, and finally, the average value was presented in Table 6.

As shown in Table 6, if the distance is fixed, increasing the voltage from 15 to 20 kV increases the diameter of PCL/SF/A nanofibers from 92.8 ± 1.4 nm to 99.1 ± 1.9 nm. In this case, there is a direct relationship between nanofiber diameter and voltage at a constant distance. If the voltage is fixed to 20 kV, increasing the distance from 15 to 18 cm increases the diameters of nanofibers from 99.1 ± 1.9 nm to 111.3 ± 1.2 nm. In this case, there is a direct relationship between nanofiber diameter and distance at a constant voltage. By increasing the distance, electric field power is reduced. As a result, the

electrical charge of the polymer chain will be reduced in the jet, leading to an increased diameter of nanofibers. This is compatible with the results of Misra et al.

3.2 | FTIR results

This section investigates FTIR spectra for PCL, fibroin, allicin nanofiber scaffolds, and composite scaffolds. The FTIR spectrum for PCL is shown in Figure 6 that high-frequency noise was removed after using the total variation algorithm, which was mentioned in Material and Method section as the proposed algorithm. As shown in Figure 5, the FTIR spectrum of the PCL scaffold shows the absorption bands of 2942, 2865 cm^{-1} (C-H functional group in CH2) and 1726 cm^{-1} (C=O functional groups). These peaks are characteristics of PCL. Considering the chemical formula of PCL and the results of reports by other researchers in [44, 45], these links are present in PCL. Therefore, these results are confirmed and are consistent with the results [44, 45] for PCL (1772 cm^{-1} for C=O functional group). The spectrum of fibroin nanofibers (Figure 5b) shows peaks at 3297, 2943, 1641, 1551, and 1238 cm^{-1}. Also, Figure 6 shows that this wavenumber can be attributed to a specific bond. These peaks represent the first type of amine NH, C-H in Ch2, C=O, C=O, and C-N, respectively. As the results show, all the bonds are compatible with the chemical formula of silk fibroin. In studies [44, 45] for silk fibroin, 1625, 1231, and 1520 cm^{-1} are, respectively, attributed to tensible vibration of C=O bound (amide I), bending vibration of NH bond (amid II), and combination of NH and C-N vibrations (amid III). The results of this study and previous works are compatible. In the third section, FTIR spectra are presented for allicin in Figure 6c. As shown in Figure 6, the FTIR spectrum of allicin shows 718, 1633, 3339, 1421, 1633, 1215, 914, 984, and 1633 cm^{-1}, which are attributed to functional groups of C-C, O-H, O-H, C-OH, C=C. As indicated in the chemical formula of allicin, these functional groups are present. Therefore, they are correctly identified [46]. Figure 6d shows the FTIR spectrum for PCL scaffolds that demonstrates absorption bands at 2865 cm^{-1} (C-H functional group in CH2), 1726 cm^{-1} (C=O functional groups), and 732 cm^{-1} (C-C functional groups). At the same time, the FTIR spectrum of fibroin nanofibers presents peaks at 3297 cm^{-1}
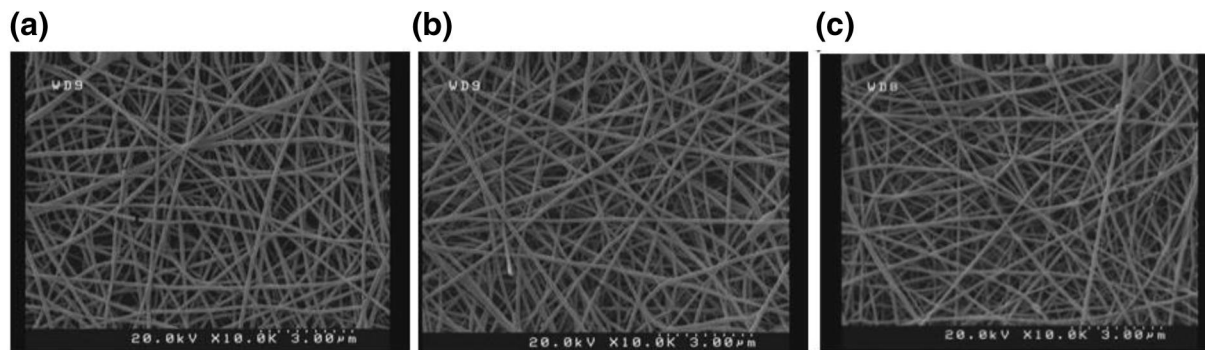
FIGURE 4 SEM images related to PCL/SF nanofibers with various distances: (a) 15 cm, (b) 15 cm, and (c) 18 cm

TABLE 5 Distance, voltage, and diameter of nanofibers for PCL/SF scaffolds

Distance (cm)	Voltage (kV)	Fibre diameter (nm) (nm)	Sample code
15	15	104.7 ± 1.1	*PCL/SF* − 15
15	15	100.2 ± 0.9	*PCL/SF* − 14
18	20	98.1 ± 2.1	*PCL/SF* − 18

(amid I in NH), 2943 cm^{-1} (C-H in CH2), 1641 cm^{-1} (C=O), 1551 cm^{-1} (C=O), and 1238 cm^{-1} (C-N), which are compatible with previous works [44] Furthermore, the results indicated that the intensity of peaks for PCL scaffolds is greater than PCL/SF in FTIR spectra, which is attributable to a higher PCL ratio. Also the results in Figure 6d show, the FTIR spectrum of the PCL/SF combination presents frequencies extracted separately from PCL and SF. These are compatible with the studies [44, 45]. Therefore, it can be seen a good compatibility between this study and previous works in [44–46]. The FTIR spectrum of PCL/SF/A is shown in Figure 6e that the FTIR spectrum illustrates peaks at 732 cm^{-1} (C-C), 961 cm^{-1} (CH=CH(trans), 1293, 1239, 1177, 1108, 1046 cm^{-1} (C-O), 1365 cm^{-1} (C-H), 2944, 2865, 1470, 1418 cm^{-1} (CH2), 1726 cm^{-1} (C=O), 1397 cm^{-1} (CH3), and 1546 cm^{-1} (C=O). As demonstrated in Figure 6, most PCL bonds and functional groups are preserved. At the same time, other bonds and functional groups that are only present in SF and allicin are reduced. This is attributable to the concentration of PCL in the scaffolds.

3.3 | Contact angle results

The contact angle results are shown in Figures 7–9 for the water drop in contact with the surface of the scaffolding. Initially, a test was performed for the PCL scaffold and its contact angle was calculated. The contact angle is shown in Figure 7. As can be seen, there are three stages from the beginning to the end. At the initial phase, the angle is 148.7°. Over time, this value decreased in stage 2 and reached 148.4°. Finally, this angle reaches 139.9° in the final stage, all of which are shown in Figure 7 a–c, respectively. The decrease in the

contact angle of the PCL nanofiber over time is due to polar ester groups in its structure as they absorb little water.

For PCL/SF scaffolds, the contact angles are shown in Figure 8 a to c. At the initial phase, the angle is 144°. Over time, this value decreased in stage 2 and reached 135.5°. Finally, this angle reaches 133.3° in the final stage.

By adding allicin to the scaffold, the contact angles are shown in Figure 9. At the initial phase, the angle is 116.5°. Over time, this value decreased 116.5° and later reached 108.3°. Finally, this angle reaches 85.5° in the final stage.

In the previous studies, the contact angle value is initially high for PCL but decreases over time to zero [47–50]. By adding SF to the PCL, the contact angle changes and is less than the contact angle of the pure PCL scaffold. The results show that the contact angle of the PCL scaffold is 139.9°. By adding SF, the contact angle reaches 133.3 in the final stage. The results of the present study are quite similar to other articles. In the study by Li et al. [48], the PCL contact angle was initially 130°, which decreased to 105° with the addition of SF. In this case, the concentration of SF is more minor than PCL. They found that, with an equal ratio of PCL/SF, the contact angle is 90°. Also, Roy et al. observed a similar reduction trend. They found that a pure PCL scaffold shows a contact angle of 130°, reaching 120° over time. The addition of SF to PCL demonstrates an initial contact angle of 80°, which reduces over time [47].

3.4 | Mechanical properties

The mechanical properties of the scaffold are shown in Figure 10. As shown in Figure 10a, the greater the force on the pure PCL scaffold, the longer the scaffold. However, at the point of 12 mm, it withstands the maximum power, and after that, the material fails. At the peak, tensile strength and Young's modulus are 0.54 MPa and 0.90 MPa, respectively. The stress versus strain diagram is the same as the force diagram in elongation that it is not here for repetitive results. The results illustrate the strain increases, so does the stress. The maximum stress at the point is 0.54 MPa, which is 60% strain. The tensile strength changes by adding SF to PCL (Figure 10-b) so that the maximum tensile strength of PCL/SF fibres decreases to 0.5 MPa. Also, as the stress increases, so does the strain that its maximum is 24.48 MPa and it declines
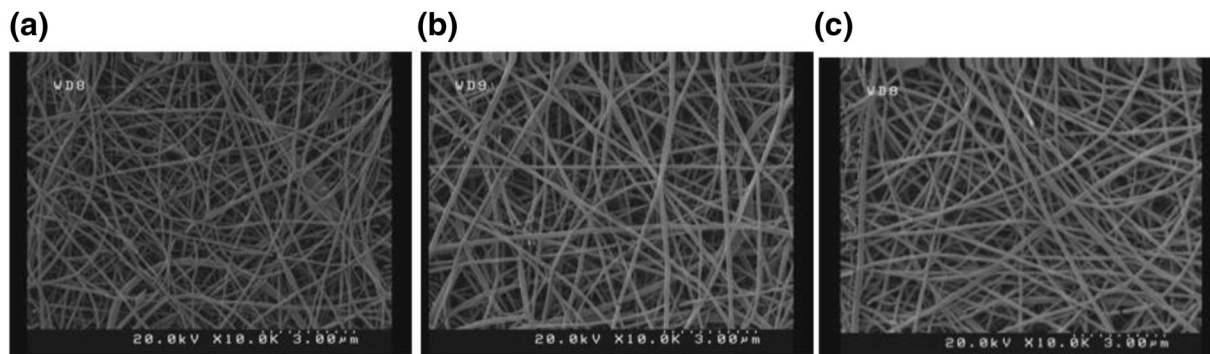
FIGURE 5 SEM images related to PCL/SF/A nanofibers with various distances: (a) 15 cm, (b) 15 cm, and (c) 18 cm

TABLE 6 Distance, voltage, and diameter of nanofibers for PCL/SF/A

Distance (cm)	Voltage (kV)	Fibre diameter (nm) (nm)	Sample code
15	15	92.8 ± 1.4	$PCL/SF/A - 15$
15	20	99.1 ± 1.9	$PCL/SF/A - 15$
18	20	111.3 ± 1.2	$PCL/SF/A - 18$
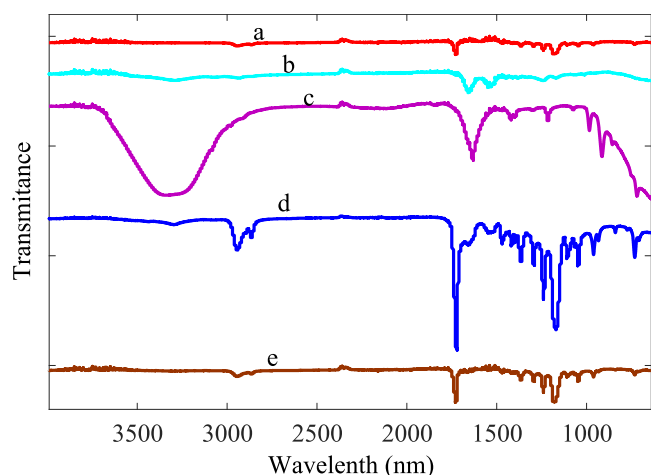
FIGURE 6 Fourier transform infrared spectra for 5 cases including (a) PCL, (b) SF, (c) (a), (d) PCL/SF, (e) PCL/SF/A after using the total variation algorithm for de-noise high-frequency noise

FIGURE 7 The contact angles associated with PCL at different times: (a) 148.7°, (b) 148.4°, and (c) 139.9°

FIGURE 8 The contact angles associated with PCL/SF scaffolds at different times: (a) 144°, (b) 135.5°, and (c) 133.3°

FIGURE 9 The contact angles associated with the addition of allicin to scaffolds at different times: (a) 116.5°, (b) 116.5°, (c) 108.3°, and (d) 85.5°

almost 50% rather than the previous case with only PCL (Table 7). In addition, the maximum Young's modulus is 2.1 MPa that occurs in extension of 5 mm. In the next step, by adding allicin to PCL/SF fibres, the plot of force to the extension decline (Figure 10c) that results in increasing Young's modulus to 5.12 MPa and decreasing stress and strain to 0.3 and 5.79 MPa, separately.

As shown in Table 7, Young's modulus of PCL is minimum (0.91 MPa). With the addition of SF to PCL, the modulus increases to 2.06 MPa, which is compatible with other reports [47–49]. Maximum Young's modulus is obtained in PCL/SF/A that is higher than PCL and PCL/SF alone. These results and the significant difference in Young's modulus and strain of
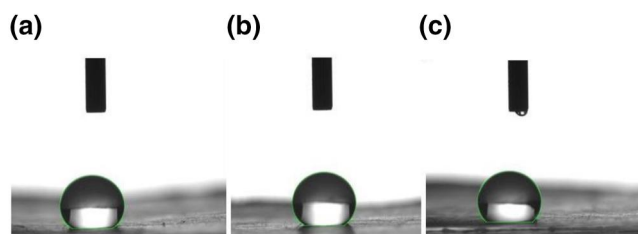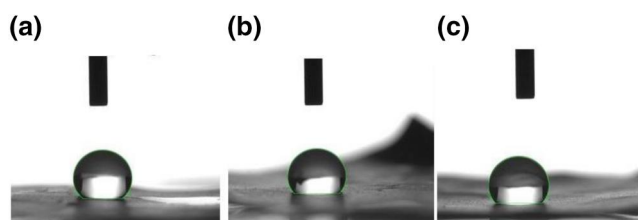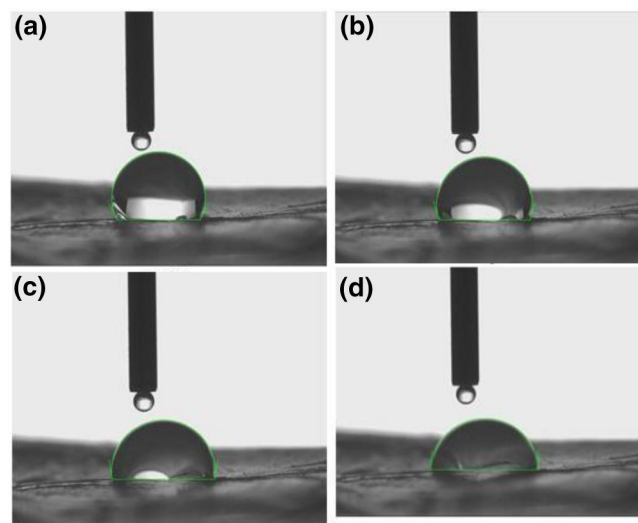
PCL with PCL/SF are due to changes in the crystal structure of SF and the formation of beta-crosslink plates by methanol [51]. Given previous work, SF's tensile and crystalline properties are mainly due to this beta structure [48, 52]. This structure can significantly impact the development of crystal microstructures of PCL fibres in PCL/SF composition [52]. Therefore, adding SF and allicin to PCL will increase the

modulus. By adding SF to PCL, the strain is reduced to the breaking point for scaffolds containing SF. Accordingly, PCL withstands high stresses at higher strains. The addition of SF and allicin reduced this amount.

3.5 | Bacterial culture test results

To measure the effect of allicin in inhibiting the growth of bacteria in the laboratory, the diameter of the growth inhibition zone was determined. After exposing the samples to Escherichia coli and Staphylococcus aureus, antibacterial properties were tested. Images of Petri dishes were taken after 24 and 48 h. The growth of inhibition zone was determined with the help of a ruler (Figure 11c). No halo was observed around the allicin-free samples. But around the sample containing allicin, a growth inhibition zone was clearly seen. This zone was so large and significant for Staphylococcus aureus that the zone for nanofibers containing allicin after 17 and 24 h was approximately 3 mm. The growth of the inhibition zone increases to more than 3 mm over time for more than 24 h. The appearance of the growth inhibition zone also proves that the allicin loaded in the PCL/SF nanofibers retains its antibacterial properties.
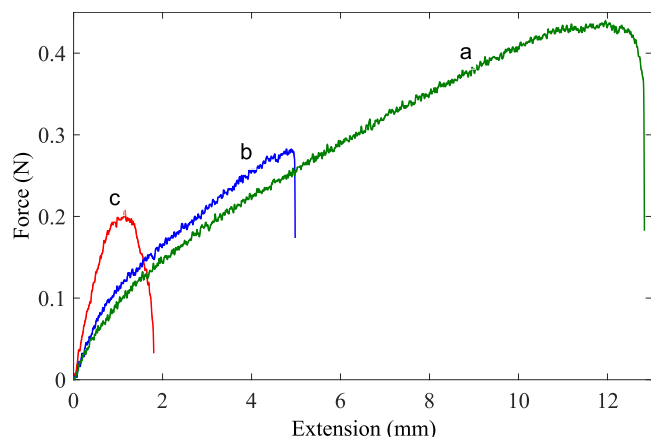

FIGURE 10 Force in terms of elongation for the scaffolds of (a) PCL, (b) PCL/SF, and (c) PCL/SF/A

**TABLE 7** Mechanical parameters for different compounds

Young's modulus (MPa)	Peak strain (%)	Peak stress (MPa)	Sample
0.91	59.78	0.54	*PCL*
2.06	24.48	0.5	*PCL/SF*
5.12	5.79	0.3	*PCL/SF/A*

3.6 | MTT result

A simple and fast method for measuring the rate of cell death is the MTT method, which is based on the formation of formazan dye by the reduction of MTT or other tetrazolium salts. By breaking the MTT tetrazolium ring by mitochondrial enzymes in living cells, insoluble purple formazan crystals are formed. The formation of these crystals indicates the activity
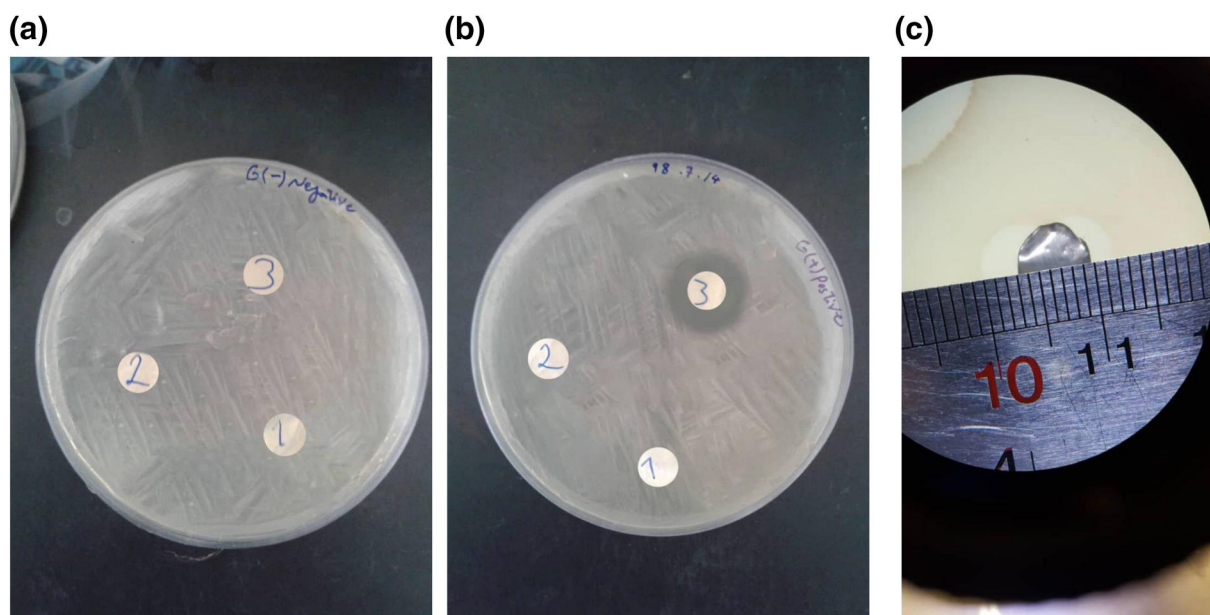
FIGURE 11 Bacterial culture test results: (a) gram-negative, (b) gram-positive. (c) The size for the diameter of the blight zone
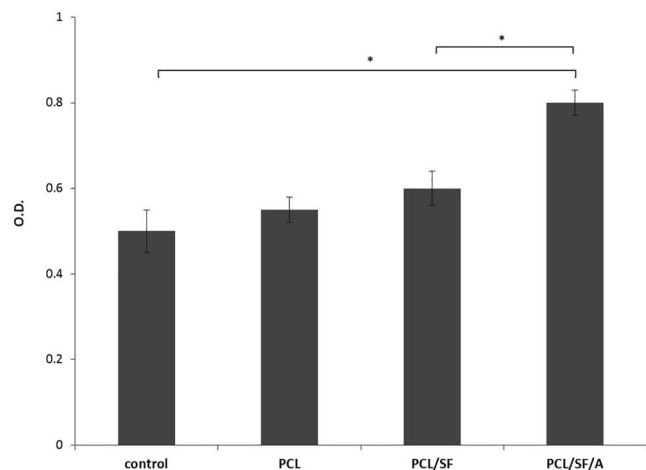
FIGURE 12 3-(4 5-dimethylthiazol-2-yl)-2 5-diphenyltetrazolium bromide test results after 24 h for the L929 fibroblast cell culture on the scaffold extract (*: $P < 0.05$)

of respiratory chain enzymes and is a measure of cell viability. By measuring the amount of absorption by spectrophotometer at specific wavelengths, the number of living cells can be determined. In the MTT test, there is no cytotoxicity about fibroblasts cultured on the scaffold extract. Compared with the control, the viability and cellular growth showed a significant increase (Figure 12).

4 | CONCLUSION

Considering the burn-related damage to the skin, it is significantly vital to repair such skin lesions. Tissue engineering is regarded as one of the methods for producing the lost tissue. In tissue engineering, it is required to provide a scaffold, which can be made through electrospinning. For the skin tissue, a scaffold material must be suitable for physical and chemical properties. In this paper, two materials, PCL and silk fibroin, are used to make nanofiber wound dressings, and allicin is used to add antibacterial properties. PCL/Fibroin/Allicin scaffold that is fabricated has the following characteristics: The SEM analysis showed that this scaffold provides smaller-diameter fibres than pure PCL and pure SF. The FTIR analysis demonstrated that functional groups of PCL, SF, and Allicin are present in the scaffold. The contact angle test showed that the scaffold has a lower contact angle than PCL, SF, and even PCL/SF, equal to 85.5°. The mechanical analysis indicated that Young's modulus of this compound is higher (2.06) than PCL and PCL/SF. Considering these characteristics, this compound is recommended for wound healing.

CONFLICT OF INTEREST
The authors declare that there is no conflict of interest.

DATA AVAILABILITY STATEMENT
The data that support the findings of this study are available from the corresponding author upon reasonable request.

PERMISSION TO REPRODUCE MATERIALS FROM OTHER SOURCES
None.

ORCID
Bita Mollaghadimi https://orcid.org/0000-0002-7161-1031

REFERENCES
1. Salamian, N., et al.: Cell attachment studies on electrospun nanofibrous PLGA and freeze-dried porous PLGA. Nano Bulletin 2(1), 130103 (2013)
2. Widmer, M.S., Mikos, A.G.: Fabrication of biodegradable polymer scaffolds for tissue engineering. InFrontiers in J Tissue Eng 1, 107–120 (1998)
3. Bhattacharya, D., Ghosh, B., Mukhopadhyay, M.: Development of nanotechnology for advancement and application in wound healing: a review. IET Nanobiotechnol. 13(8), 778–785 (2019). https://doi.org/10.1049/iet-nbt.2018.5312
4. Cheung, H.Y., et al.: A critical review on polymer-based bio-engineered materials for scaffold development. Compos. B Eng. 38(3), 291–300 (2007). https://doi.org/10.1016/j.compositesb.2006.06.014
5. Sweeney, I.R., Miraftab, M., Collyer, G.: A critical review of modern and emerging absorbent dressings used to treat exuding wounds. Int. Wound J. 9(6), 601–612 (2012). https://doi.org/10.1111/j.1742-481x.2011.00923.x
6. Jin, S.G., et al.: Mechanical properties and in vivo healing evaluation of a novel Centella asiatica-loaded hydrocolloid wound dressing. Int. J. Pharm. 490(1-2), 240–247 (2015). https://doi.org/10.1016/j.ijpharm.2015.05.058
7. Winter, G.D.: Formation of the scab and the rate of epithelization of superficial wounds in the skin of the young domestic pig. Nature 193(4812), 293–294 (1962). https://doi.org/10.1038/193293a0
8. Martín Giménez, V.M., et al.: Synthesis, physicochemical characterisation and biological activity of anandamide/-polycaprolactone nanoparticles obtained by electrospraying. IET Nanobiotechnol. 14(1), 86–93 (2020). https://doi.org/10.1049/iet-nbt.2019.0108
9. Abamor, E.S., et al.: Nigella sativa oil entrapped polycaprolactone nanoparticles for leishmaniasis treatment. IET Nanobiotechnol. 12(8), 1018–1026 (2018). https://doi.org/10.1049/iet-nbt.2018.5115
10. Ghosal, K., et al.: Structural and surface compatibility study of modified electrospun poly (-caprolactone)(PCL) composites for skin tissue engineering. AAPS PharmSciTech 18(1), 72–81 (2017). https://doi.org/10.1208/s12249-016-0500-8
11. Ghosal, K., et al.: Collagen coated electrospun polycaprolactone (PCL) with titanium dioxide (TiO2) from an environmentally benign solvent: preliminary physico-chemical studies for skin substitute. J. Polym. Res. 21(5), 1–5 (2014). https://doi.org/10.1007/s10965-014-0410-y
12. Ghosal, K., et al.: Electrospinning tissue engineering and wound dressing scaffolds from polymer-titanium dioxide nanocomposites. Chem. Eng. J. 358, 1262–1278 (2019). https://doi.org/10.1016/j.cej.2018.10.117
13. Ghosal, K., et al.: Electrospinning over solvent casting: tuning of mechanical properties of membranes. Sci. Rep. 8(1), 1–9 (2018). https://doi.org/10.1038/s41598-018-23378-3
14. Khunová, V., et al.: Antibacterial electrospun polycaprolactone nanofibers reinforced by halloysite nanotubes for tissue engineering. Polymers 14(4), 746 (2022). https://doi.org/10.3390/polym14040746
15. Zhou, L., et al.: Electrospun chitosan oligosaccharide/polycaprolactone nanofibers loaded with wound-healing compounds of Rutin and Quercetin as antibacterial dressings. Int. J. Biol. Macromol. 183, 1145–1154 (2021). https://doi.org/10.1016/j.ijbiomac.2021.05.031
16. Jia, M., et al.: Polydopamine coated lithium lanthanum titanate in bilayer membrane electrolytes for solid lithium batteries. ACS Appl. Mater. Interfaces 12(41), 46231–46238 (2020). https://doi.org/10.1021/acsami.0c14211
17. Qi, L., et al.: Unidirectional water-transport antibacterial trilayered nanofiber-based wound dressings induced by hydrophilic-hydrophobic gradient and self-pumping effects. Mater. Des. 201, 109461 (2021). https://doi.org/10.1016/j.matdes.2021.109461

18. Jirkovec, R., et al.: Preparation of a hydrogel nanofiber wound dressing. Nanomaterials 11(9), 2178 (2021). https://doi.org/10.3390/nano11092178

19. Fatehi, P., Abbasi, M.: Medicinal plants used in wound dressings made of electrospun nanofibers. J Tissue Eng & Regener Med 14(11), 1527–1548 (2020). https://doi.org/10.1002/term.3119

20. Jung, S.M., et al.: Spirulina-PCL nanofiber wound dressing to improve cutaneous wound healing by enhancing antioxidative mechanism. J. Nanomater. 2016, 1–10 (2016). https://doi.org/10.1155/2016/6135727

21. Leite, M.L., et al.: Development of fibronectin-loaded nanofiber scaffolds for guided pulp tissue regeneration. J. Biomed. Mater. Res. B Appl. Biomater. 109(9), 1244–1258 (2021). https://doi.org/10.1002/jbm.b.34785

22. Perumal, G., et al.: Synthesis of magnesium phosphate nanoflakes and its PCL composite electrospun nanofiber scaffolds for bone tissue regeneration. Mater. Sci. Eng. C 109, 110527 (2020). https://doi.org/10.1016/j.msec.2019.110527

23. Wang, J., et al.: Enhancement of Schwann cells function using graphene-oxide-modified nanofiber scaffolds for peripheral nerve regeneration. ACS Biomater. Sci. Eng. 5(5), 2444–2456 (2019). https://doi.org/10.1021/acsbiomaterials.8b01564

24. Kim, B.J., et al.: A ccelerated skin wound healing using electrospun nanofibrous mats blended with mussel adhesive protein and poly-caprolactone. J. Biomed. Mater. Res. 105(1), 218–225 (2017). https://doi.org/10.1002/jbm.a.35903

25. Venugopal, J., Ramakrishna, S.: Applications of polymer nanofibers in biomedicine and biotechnology. Appl Biochem & Biotechnol 125(3), 147–157 (2005). https://doi.org/10.1385/abab:125:3:147

26. Jebali, A., et al.: Antimicrobial activity of nanocellulose conjugated with allicin and lysozyme. Cellulose 20(6), 2897–2907 (2013). https://doi.org/10.1007/s10570-013-0084-3

27. Sardari, K., et al.: Macroscopic aspects of wound healing (contraction and epithelialisation) after topical administration of allicin in dogs. Comp. Clin. Pathol. 15(4), 231–235 (2006). https://doi.org/10.1007/s00580-006-0634-2

28. Banerjee, S.K., Maulik, S.K.: Effect of garlic on cardiovascular disorders: a review. Nutr. J. 1(1)4 (2002). https://doi.org/10.1186/1475-2891-1-4

29. Bakri, I.M., Douglas, C.W.I.: Inhibitory effect of garlic extract on oral bacteria. Arch. Oral Biol. 50(7), 645–651 (2005). https://doi.org/10.1016/j.archoralbio.2004.12.002

30. Curtis, H., et al.: Broad-spectrum activity of the volatile phytoanticipin allicin in extracts of garlic (Allium sativum L.) against plant pathogenic bacteria, fungi and Oomycetes. Physiol. Mol. Plant Pathol. 65(2), 79–89 (2004). https://doi.org/10.1016/j.pmpp.2004.11.006

31. Gao, Y., et al.: Allicin enhances cytotoxicity of CPT-11 to colon cancer LoVo cell in vitro. Zhongguo Zhong Yao za zhi= Zhongguo zhongyao zazhi= China journal of Chinese materia medica 34(23), 3092–3095 (2009)

32. Juris, S., et al.: Biodegradable polysaccharide gels for skin scaffolds. J. Biomaterials Nanobiotechnol. 2(03), 216–225 (2011). https://doi.org/10.4236/jbnb.2011.23027

33. Fletcher, J., et al.: Pressure ulcers and hydrocolloids. Made easy. Wounds Int [Intenet] 2(4) (2011)

34. Abbasi-Kesbi, R., Nikfarjam, A.: Denoising MEMS accelerometer sensors based on L2-norm total variation algorithm. Electron. Lett. 53(5), 322–324 (2017). https://doi.org/10.1049/el.2016.3811

35. Abbasi-Kesbi, R., Nikfarjam, A., Memarzadeh-Tehran, H.: A patient-centric sensory system for in-home rehabilitation. IEEE Sensor. J. 17(2), 524–533 (2016). https://doi.org/10.1109/jsen.2016.2631464

36. Abbasi-Kesbi, R., Nikfarjam, A.: A miniature sensor system for precise hand position monitoring. IEEE Sensor. J. 18(6), 2577–2584 (2018). https://doi.org/10.1109/jsen.2018.2795751

37. Akhavanhezaveh, A., Abbasi-Kesbi, R.: Diagnosing gait disorders based on angular variations of knee and ankle joints utilizing a developed wearable motion sensor. Healthcare Technol Lett 8(5), 118–127 (2021). https://doi.org/10.1049/htl2.12015

38. Jaloli, M., et al.: A proposed algorithm for the detection of thyroid cancer based on image processing. J Bioeng Res 1(3), 7–14 (2019)

39. Abbasi-Kesbi, R., Valipour, A., Imani, K.: Cardiorespiratory system monitoring using a developed acoustic sensor. Healthcare Technol LettLett 5(1), 7–12 (2018). https://doi.org/10.1049/htl.2017.0012

40. Abbasi-Kesbi, R., Nikfarjam, A., Akhavan Hezaveh, A.: Developed wearable miniature sensor to diagnose initial perturbations of cardiorespiratory system. Healthcare Technol Lett 5(6), 231–235 (2018). https://doi.org/10.1049/htl.2018.5027

41. Fathi, M., et al.: A machine learning approach based on SVM for classification of liver diseases. Biomed. Eng.: Appl, Basis & Commun 32(03), 2050018 (2020). https://doi.org/10.4015/s1016237220500180

42. Abbasi-Kesbi, R., Asadi, Z., Nikfarjam, A.: Developing a wireless sensor network based on a proposed algorithm for healthcare purposes. Biomedi Eng Lett 10(1), 163–170 (2020). https://doi.org/10.1007/s13534-019-00140-w

43. Abbasi-Kesbi, R., Memarzadeh-Tehran, H., Deen, M.J.: Technique to estimate human reaction time based on visual perception. Healthcare Technol Lett 4(2), 73–77 (2017). https://doi.org/10.1049/htl.2016.0106

44. Zahedi, P., et al.: A review on wound dressings with an emphasis on electrospun nanofibrous polymeric bandages. Polym. Adv. Technol. 21(2), 77–95 (2010). https://doi.org/10.1002/pat.1625

45. Horkan, L., Stansfield, G., Miller, M.: An analysis of systematic reviews undertaken on standard advanced wound dressings in the last 10 years. J. Wound Care 18(7), 298–304 (2009). https://doi.org/10.12968/jowc.2009.18.7.43113

46. Ng, S.F., Jumaat, N.: Carboxymethyl cellulose wafers containing antimicrobials: a modern drug delivery system for wound infections. Eur. J. Pharmaceut. Sci. 51, 173–179 (2014). https://doi.org/10.1016/j.ejps.2013.09.015

47. Roy, T., et al.: Core-shell nanofibrous scaffold based on polycaprolactone-silk fibroin emulsion electrospinning for tissue engineering applications. Bioengineering 5(3), 68 (2018). https://doi.org/10.3390/bioengineering5030068

48. Li, L., et al.: Electrospun poly (e-caprolactone)/silk fibroin core-sheath nanofibers and their potential applications in tissue engineering and drug release. Int. J. Biol. Macromol. 49(2), 223–232 (2011). https://doi.org/10.1016/j.ijbiomac.2011.04.018

49. Lee, H., Jang, C.H., Kim, G.H.: A polycaprolactone/silk-fibroin nanofibrous composite combined with human umbilical cord serum for subacute tympanic membrane perforation; an in vitro and in vivo study. J. Mater. Chem. B 2(18), 2703–2713 (2014). https://doi.org/10.1039/c4tb00213j

50. Fu, W., et al.: Electrospun gelatin/PCL and collagen/PLCL scaffolds for vascular tissue engineering. Int. J. Nanomed. 92335 (2014). https://doi.org/10.2147/ijn.s61375

51. Noishiki, Y., et al.: Mechanical properties of silk fibroin–microcrystalline cellulose composite films. J. Appl. Polym. Sci. 86(13), 3425–3429 (2002). https://doi.org/10.1002/app.11370

52. Bazilevsky, A.V., Yarin, A.L., Megaridis, C.M.: Co-electrospinning of core-shell fibers using a single-nozzle technique. Langmuir 23(5), 2311–2314 (2007). https://doi.org/10.1021/la063194q